Growth dynamics of SiGe nanowires by the Vapour Liquid Solid method and its impact on SiGe/Si axial heterojunction abruptness

J. L. Pura,[a]* *P. Periwal,*[b] *T. Baron,*[b] *J. Jiménez* [a]

a. GdS Optronlab, Dpt. Física de la Materia Condensada, ed. LUCIA Universidad de Valladolid, Paseo de Belén 19, 47011 Valladolid, Spain

b. University Grenoble Alpes, LTM, F-38000 Grenoble, France and CNRS, LTM, F-38000 Grenoble, France

* Email: jlpura@fmc.uva.es

Keywords: SiGe, Si, nanowires, heterojunctions, VLS, growth dynamics

Abstract

The Vapour Liquid Solid (VLS) method is by far the most extended procedure for bottom-up nanowire growth. This method also allows for the manufacture of nanowire axial heterojunctions in a straightforward way. To do this, during the growth process the precursor gases are switched on/off to obtain the desired change in the nanowire composition. Using this technique axially heterostructured nanowires can be grown, which are crucial for the fabrication of electronic and optoelectronic devices. SiGe/Si nanowires are compatible with Complementary Metal Oxide Semiconductor (CMOS) technology, this improves their versatility and the possibility of integration with the current electronic technologies. Abrupt heterointerfaces are fundamental for the development and correct operation of electronic and optoelectronic devices. Unfortunately, VLS growth of SiGe/Si heterojunctions does not provide abrupt transitions because of the high solubility of group IV semiconductors in Au, with the corresponding reservoir effect that precludes the growth of sharp interfaces. In this work, we studied the growth dynamics of SiGe/Si heterojunctions based on already developed models for VLS growth. A composition map of the Si-Ge-Au liquid alloy is proposed to better understand the impact of the growing conditions on the nanowire growth process and the heterojunction formation. The solution of our model provides heterojunction profiles in good agreement with experimental measurements. Finally, the in-depth study of the composition map provides a practical approach to reduce drastically the heterojunction abruptness by reducing the Si and Ge concentrations in the catalyst droplet. This converges with previous approaches that use catalysts aiming to reduce the solubility of the atomic species. This analysis opens new paths to reduce the heterojunction abruptness using Au catalysts, but the model can be naturally extended to other catalysts and semiconductors.

1. Introduction

Heterostructured semiconductor nanowires (NWs) are the building blocks of the future nanodevices. In particular, axially heterostructured NWs promise new devices in electronics,[1,2] photonics[3] and thermoelectric conversion,[4] among other applications. A key issue concerns the control of the heterojunctions, which is crucial to the performance of those devices. Generally, one needs abrupt interfaces for the optimal operation of the devices,[5] especially those that rely on quantum wells and quantum confinement effects.[6,7]

Most semiconductor NWs are grown in a bottom up approach by means of the Vapour Liquid Solid (VLS) technique.[8] In VLS the constituent elements of the NW are incorporated to a metallic droplet (catalyst) forming a supersaturated liquid alloy, from which epitaxial layer by layer deposition at the solid (NW)/ liquid (catalyst droplet) interface takes place. The growth rate is governed by the difference of chemical potentials of the constituent elements between their liquid and solid phases. Axially heterostructured NWs are very promising for growing complex devices with multi-junctions,[9] suitable for one-dimensional electronic and optoelectronic devices. Axially heterostructured NWs are manufactured by switching off/on the vapour phase reactants during the VLS growth.[10] These heterostructured NWs have been grown with different combinations of III-V compounds, III-Vs and Si, and also group IV semiconductors, like Si/Ge and Si/SiGe heterojunctions. While sharp heterointerfaces have been reported for III-V heterostructured NWs,[11,12] group IV NW heterointerfaces are more gradual, forming a relatively broad compositionally graded transition between the two extreme compositions of the NW.[13] However, atomically abrupt Si/SiGe interfaces have been recently achieved by using other methods or catalysts like Sn catalysed solvent vapour (SVG) growth (VLS) [14] or Au/Al [15] and Ag/Au [16] catalysed vapour solid solid (VSS) growth. Such a different

behaviour between III-V and group IV axially heterostructured NWs has been related to the different solubilities of the constituent elements in the metallic droplet.[17] The high solubility of Ge and Si in Au results in a reservoir effect of those atomic species in the catalyst droplet. After switching off the reactant gas source, the remaining atomic species still continue to be deposited until they reach equilibrium. As a result, the deposition of the remaining atomic species should prevent step-like interfaces. For III-V semiconductors, the low solubility of the column V elements in the catalysts droplet suppresses the reservoir effect by a great amount, which will result in much sharper heterointerfaces.

In recent work, we have shown that axially heterostructured Si/SiGe NWs present potential qualities for photon engineering. Indeed, a strong enhancement of the optical absorption/ scattering at the heterojunction of these NWs was observed by Raman spectroscopy.[18,19] Electromagnetic calculations suggest that the absorption/scattering by the axially heterostructured NWs can be tuned by engineering the heterointerfaces. This opens an interesting way for photon harvesting based on the control of the composition of axial NW heterointerfaces.

Heterostructured Si/SiGe NWs present two different heterointerfaces: SiGe/Si and Si/SiGe in growth direction, labelled trailing and leading interfaces, respectively. The interface abruptness refers to the width of the transition region between the two homogeneous segments of the NW. The growth mechanisms for axially heterostructured NWs are far from being fully understood, in spite of the existence of a few models that roughly fit the scarce experimental data concerning the abruptness of the axial NW heterojunctions. We present herein an analysis of the growth of both trailing and leading heterointerfaces in axially heterostructured Si/SiGe NWs. Our study is based on already

developed models, from which we establish a full composition growth map describing the formation of the heterointerfaces in Au catalysed VLS Si/SiGe NWs.

2. Growth Model

Alloyed SiGe NWs are grown by the VLS method using SiH_4 and GeH_4 vapour reactants. The reactants diffuse onto the Au droplet surface and dissociate releasing the constituents in the liquid droplet, then they diffuse towards the liquid-solid interface. The growth of axial heterointerfaces is obtained by switching-off/on the gas sources of the reactants according to the desired compositional change. However, a sudden switch of the reactant flux is not synonymous of an abrupt interface, because the remaining atomic species solved in the droplet at the instant of the switch-off are still in supersaturation and will keep being deposited at the liquid-solid interface. As the heterojunction starts growing a compositionally graded transition takes place as far as the excess atoms in the droplet are deposited and progressively replaced in the metallic droplet by the constituent atoms forming the next NW segment.

A discussion about the abruptness of the heterointerfaces and the consequences of the reservoir effect in the catalyst droplet can be found in [20,21]. However, the analysis of the heterointerfaces and the growth conditions for controlling them is still a matter of controversy. Our model is based on layer-by-layer growth without considering details about the layer nucleation and the monolayer growth dynamics. For detailed analyses of these aspects see Refs. [22–26]. Here, we will focus on gold catalysts, which are by far the most commonly used. Anyway, the model can be easily extended to other metals. For the development of the model we have applied the growth principles described in Refs. [17,20].

In this model the growth rate of a monolayer (ML) at the solid-liquid interface is proportional to the difference in the chemical potentials of the liquid and the solid alloy phases. Therefore, the deposition rates of pure Ge and pure Si can be written as

$$v_{Ge}^{(i)} = \Gamma_{Ge}\Delta\mu_{Ge}^{(i)};\ v_{Si}^{(i)} = \Gamma_{Si}\Delta\mu_{Si}^{(i)} \quad (1)$$

Where $\Delta\mu_{Ge(Si)}$ is the difference between the chemical potentials of the liquid and solid phases for Ge and Si, respectively. The kinetic parameters, Γ_{Ge} and Γ_{Si}, are related to the equilibrium concentration of the corresponding atomic species, therefore, they are basically determined by the solubility of each element in Au. According to this, we can define a parameter $B = \Gamma_{Si}/\Gamma_{Ge}$, which should be smaller than 1 because of the higher solubility of Ge than Si in Au.

The discrete index *i* numbers the successive monolayers forming the interface, because in the heterointerface the Ge concentration is gradually varying from each ML to the next one. As Si and Ge concentrations in the catalyst droplet are changing, the composition of each ML will depend on the composition of the precedent one. The chemical potentials of the solid phase and the kinetic parameters might slightly vary depending on the ML position at the heterointerface, because of the concentration variation. In our calculations, we assume that both parameters do not depend on the ML position for a sake of simplicity, but also because of the lack of data about its dependence with the composition.

Accordingly, the Ge concentration of the *i*-th layer can be calculated as:

$$x_i = \frac{v_{Ge}^{(i)}}{v_{Ge}^{(i)} + v_{Si}^{(i)}} = \frac{\Gamma_{Ge}\Delta\mu_{Ge}^{(i)}}{\Gamma_{Ge}\Delta\mu_{Ge}^{(i)} + \Gamma_{Si}\Delta\mu_{Si}^{(i)}} = \frac{1}{1 + B\dfrac{\Delta\mu_{Si}^{(i)}}{\Delta\mu_{Ge}^{(i)}}} \quad (2)$$

The chemical potentials are calculated according to the Glas model[27] for the III-V NW growth based on the Stringfellow ternary phase diagrams,[28] and adapted to the SiGe alloy system as:

$$\Delta\mu_k^{(i)} = \mu_k^{pL} + k_B T \ln C_k^{(i)} + \omega_{kj}\left[C_j^{(i)}\right]^2 + \omega_{kAu} C_{Au}^2 + C_j^{(i)} C_{Au}\left(\omega_{kj} + \omega_{kAu} - \omega_{jAu}\right) - \mu_k^S \quad (3)$$

Where C_{Si} and C_{Ge} are the Si and Ge concentrations in the liquid droplet, while $C_{Au} = (1 - C_{Si} - C_{Ge})$ is the Au concentration. μ_k^{pL} and μ_k^S are, respectively, the chemical potentials of the pure liquid and pure solid phases. The ω parameters account for the interatomic interactions in the liquid phase and are given by:

$$\omega_{\alpha\beta} = \frac{1}{N_A}\frac{V_\alpha V_\beta}{C_\alpha V_\alpha + C_\beta V_\beta}\left[\left(\delta_\alpha - \delta_\beta\right)^2 - F\frac{\left(\chi_\alpha - \chi_\beta\right)^2}{(V_\alpha V_\beta)^{\frac{1}{2}}}\right] \quad (4)$$

where $V_\alpha = M_\alpha/\rho_\alpha N_A$ is the molar volume and M_α, ρ_α, χ_α, δ_α denote molar mass, density, Pauling electronegativity, and Hildebrand solubility parameter of species α and β , respectively, N_A is the Avogadro number, and $F = 1.256 \times 10^5$ if all quantities are in SI units. The solubility parameter δ_α is taken as: $\delta_\alpha = [(\Delta H_\alpha^{at} - RT)/V_\alpha]^{1/2}$, where ΔH_α^{at} is the molar heat of atomization. All other coefficients except μ_k^S can be found in reference books. [27,22,29] The numerical values of the parameters used in our calculations can be found in the supporting information S1. The unknown values of $\mu_{Si/Ge}^{pL}$ and $\mu_{Si/Ge}^{S}$ were fixed by the conditions that the corresponding difference of chemical potential is zero at the equilibrium concentration of Si/Au and Ge/Au alloys respectively. Therefore, we put

$\Delta\mu_{Si} = 0$ at $C_{Ge} = 0$, $C_{Si} = 0.22$, $C_{Au} = 0.78$, and $\Delta\mu_{Ge} = 0$ at $C_{Si} = 0$, $C_{Ge} = 0.35$ and $C_{Au} = 0.65$ at the growth temperature T = 450 °C.[29] Thus $\mu^{S}_{Si/Ge}$ are approximately taken as independent of i, i.e. independent of the layer composition.

The heterointerface width in a transition from $Si_{(1-x)}Ge_x$ to Si is calculated as the distance between the monolayers with Ge concentrations $x = (1-\delta)x_0$ and $x = \delta x_0$, for $\delta = 0.1$, where x_0 is the Ge concentration of the homogeneous SiGe segment.

By solving this model we can establish a complete description of the growth of both heterointerfaces, leading and trailing, allowing to select the experimental growth conditions required for obtaining a predefined heterointerface abruptness.

Results

In order to understand the growth of the interfaces we will analyse the growth dynamics in a continuous compositional change. First, we start by studying the Ge concentration of the NW solid phase *x*, as a function of Si and Ge concentrations in the liquid droplet, C_{Si} and C_{Ge}, Eq. 2. A 3D representation of this magnitude can be seen in Figure 1.

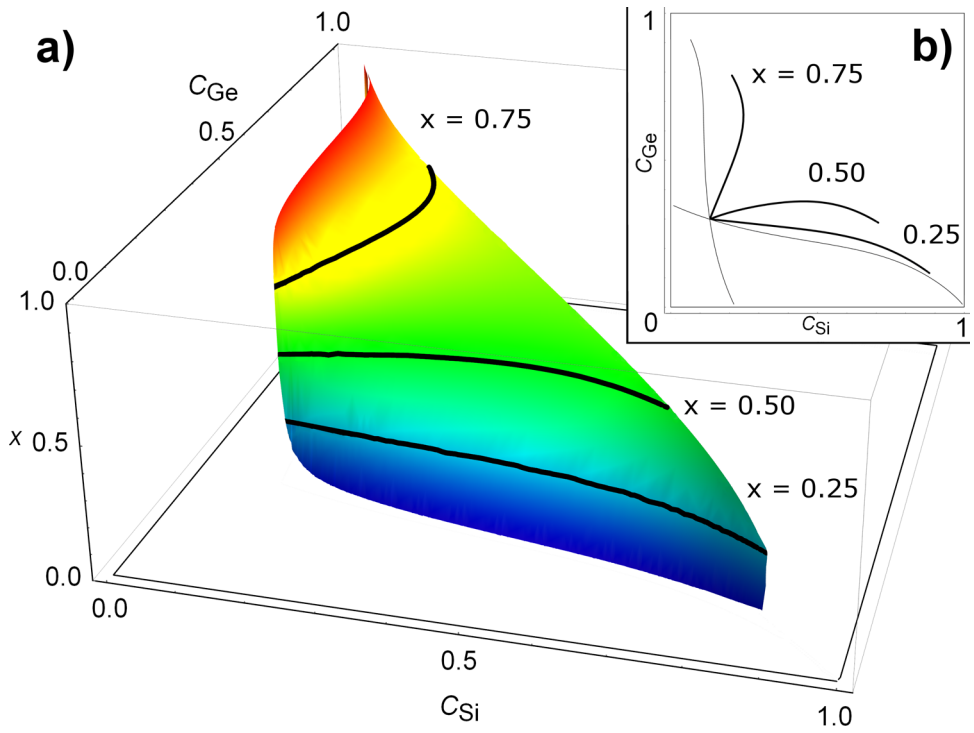

Figure 1. a) 3D map of the NW growing composition, x, as a function of Si and Ge concentrations in the Au catalyst droplet. The black curves represent the pairs of concentrations resulting in the same solid phase composition *x*, three of them are plotted as an example: $x = 0.25$, $x = 0.50$ and $x = 0.75$ from bottom to top. b) Plane projection of Figure 1a, showing the previously mentioned curves, and the limiting curves for x = 0 and x = 1 (gray curves).

Figure 1 shows the growth concentration of the solid phase, x, as a function of both Si and Ge concentrations in the liquid droplet. We can observe two limiting regions: one for *x* approaching 1 (red colour in the 3D plot), which corresponds to low C_{Si}, close to the pure Ge NW growth. The other limiting region appears for *x* approaching 0 (blue colour in the 3D plot), which corresponds to low C_{Ge} values approaching the pure Si growth. These two limiting regions are described by two curves in the (C_{Si}, C_{Ge}) plane, corresponding to the liquid-solid equilibrium for Si and Ge, respectively. These curves can be easily computed by finding the concentrations at which $\Delta\mu_{Si} = 0$, no Si deposition

(x = 1 in the solid phase); and $\Delta\mu_{Ge}$ = 0, no Ge deposition (x = 0 in the solid phase). Between these two limiting curves there is a curve for each growing composition ranging from 0 to 1. These curves represent the degenerated pairs of Si and Ge concentrations in the liquid phase that result in the growth of the same Ge concentration in the solid phase. Three of these curves are plotted in Figure 1 as an example (x = 0.25, 0.50 and 0.75).

Figure 2 shows a projection of Figure 1 on the C_{Ge}-C_{Si} plane where we can see the two equilibrium curves as well as the curve for x = 0.5, providing us with a composition map for the growth of the heterointerface of a $Si_{1-x}Ge_x$/Si NW for a concentration x = 0.5, which will be used as an example. It is important to note that the Au droplet remains in liquid state regardless of the Si and Ge concentrations, also, the total number of Au atoms in the droplet is assumed to remain unchanged during the growth process. Remind that any significant Au losses in the catalysts droplet will modify the growth dynamics and induce NW diameter changes.

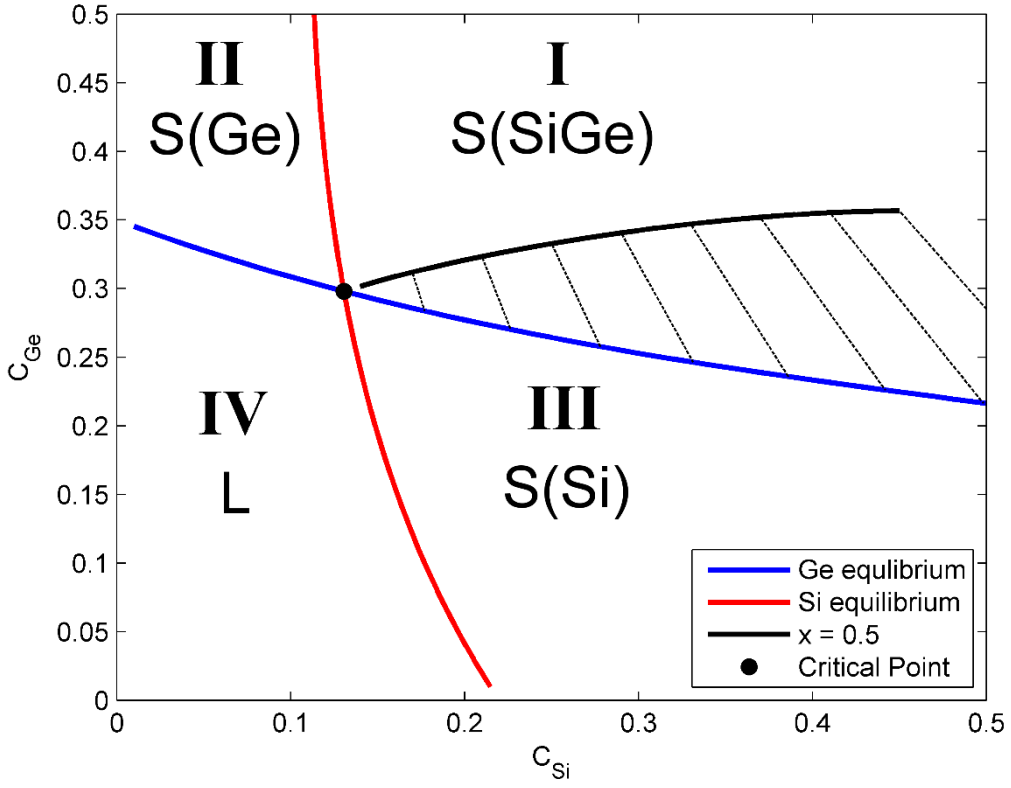

Figure 2. Composition map of the Au/Si/Ge alloy, as a function of Si and Ge concentrations in the liquid phase. Note that the region of interest is that of $C_{Si} + C_{Ge} \leq 1$, however only the region near the critical point is represented since it contains all the relevant information.

The two curves corresponding to $\Delta\mu_{Si} = 0$ (red) and $\Delta\mu_{Ge} = 0$ (blue) define four regions in the (C_{Si}, C_{Ge}) plane, numbered I to IV. Region I is the region of interest for the heterostructured NW growth purposes, where the liquid Au/Si/Ge alloy (L) coexists with the $Si_{(1-x)}Ge_x$ solid phase ($S(Si_{(1-x)}Ge_x)$) of a certain concentration *x* ($L + S(Si_{(1-x)}Ge_x)$). In region II $\Delta\mu_{Si} < 0$, then Si tends to dissolve in the droplet and cannot be deposited in the solid phase, therefore, only the Ge NWs can be grown for such low Si concentration (L + S(Ge)). Region III is the analogue to region II, but interchanging Si and Ge roles (L + S(Si)). Finally, in region IV the liquid phase is thermodynamically more stable for both Si and Ge, and there is no nucleation of the solid phase (L). This plot conforms a composition map for the growth of $Si_{(1-x)}Ge_x$ NWs at 450ºC.

It is important to note the existence of a critical point, defined by the intersection of the two equilibrium curves, which is located at coordinates (C_{Si}, C_{Ge}) ~ (0.1307, 0.2980). This point corresponds to the perfect equilibrium between liquid and solid phases of both atomic species. The simultaneous equilibrium of Si and Ge implies the equilibrium of two phases: the $Si_{(1-x)}Ge_x$ solid phase for any composition, *x*, and the liquid Au/Si/Ge alloy. According to this, fast compositional transitions shall occur with only little changes in the concentration when the system is in the vicinity of this critical point. This will directly affect the interfacial abruptness as we will see later on.

Now, we will analyse the two types of heterointerfaces: the trailing one, in which SiGe is growing and the Ge flow is switched off, and the leading one in which pure Si is growing and the nominal Ge flow is restored.

3.1 Trailing HJ

The so called trailing HJ profile corresponds to the heterointerface resulting from the transition from $Si_{(1-x)}Ge_x$ to pure Si. It is frequently claimed that the trailing HJ should be relatively extended because of the reservoir effect due to the high solubility of Ge in liquid Au. However, it should be noted that Ge stops its deposition once the Ge concentration in the droplet is under the saturation value. In this context, pure Si means that traces of Au and/or Ge might be present in the Si segment by stochastic incorporation, but in very low concentrations, < 1%, which do not alter the Si structure. The exact concentration of Ge in the Si segment is not easy to calculate; however, we can make a rough estimation assuming that the adsorption and desorption probabilities of the Ge atoms on the solid phase are similar once the Ge is under saturation in the metal droplet. In this case, we can expect, on average, the incorporation of one Ge atom per bilayer as an upper bound, which results in a Ge/Si concentration ratio around 10^{-5} for a NW with 100 nm diameter.

According to the composition map of Figure 2, during the growth of the homogeneous $Si_{(1-x)}Ge_x$ segment the system is located at a certain point of the curve corresponding to concentration x (black line in Figure 2 for $x = 0.5$). The exact point on such curve will depend on the growth conditions, i.e. on the amount of Si and Ge dissolved in the Au droplet. This amount is determined by the Si and Ge fluxes and also their corresponding solubilities in the catalysts droplet, which depend on temperature and pressure. Once the Ge source is switched-off, the Ge in the catalysts droplet will keep being deposited, but no more Ge is fed into the droplet from the vapour phase. This will progressively reduce the Ge concentration in the droplet, following one of the dashed curves of Figure 2, until

the Ge equilibrium curve is reached (blue curve in Figure 2), beyond this point no more Ge is deposited. On the other hand, the relative Si concentration will slightly increase during the transition, because of the reduction of the total amount of Ge atoms in the droplet, which are progressively replaced by Si atoms. Once the Ge equilibrium concentration is reached the Ge deposition stops, even if there is still Ge in the catalyst droplet; this dynamics would result in a trailing HJ sharper than expected if Ge in the droplet was exhausted. In fact, the analysis of the catalyst droplet still evidences the presence of Ge, once the Ge source was switched-off, and the Si segment was grown. [30]

The droplet composition dynamics can be summarized in the following two equations

$$C_{Ge}^{i+1} = C_{Ge}^{i} - x_i(C_{Si}^{i}, C_{Ge}^{i})\frac{3h}{d} \quad (5)$$

$$C_{Si}^{i+1} = C_{Si}^{i}\frac{(1 - C_{Ge}^{i+1})}{(1 - C_{Ge}^{i})} \quad (6)$$

Where h is the height of one SiGe monolayer ≈ 0.5 nm, d is the NW diameter, x_i the Ge composition of the i-th monolayer, and C_{Si} and C_{Ge} the Si and Ge concentrations on the liquid droplet. Eq. 5 describes the change in C_{Ge} as Ge is being deposited, Eq. 6 accounts for the change in C_{Si} as a result of the change in C_{Ge}. Given the initial conditions of the system (C_{Si}, C_{Ge}), the iterative solution of these two equations provides the composition profile of the transition from SiGe to Si. Figure 3 shows a series of trailing HJ profiles from $x = 0.5$ ($Si_{0.5}Ge_{0.5}$ NW segment) to $x = 0$ (Si segment) calculated for different starting points along the x = 0.5 curve (black line in Figure 2), B = 0.5 and d =100 nm. The calculated heterointerface composition profiles correspond to the transitions from the black line of Figure 2 to the Ge equilibrium curve (blue), each process takes place along

one of the black dashed lines in Figure 2. One can observe that the abruptness of the heterointerface strongly depends on the starting point over the black line, which is determined by the growth conditions, mainly Si and Ge fluxes, however all the conditions derived here will depend on the selected temperature and pressure. The HJ becomes broader as the starting point moves away from the critical point. This behaviour shows a way to tailor the HJ sharpness, it also shows the possibility of creating abrupt SiGe/Si heterointerfaces with extensions of only a few nanometres by adjusting the growth conditions as closer as possible to the critical point during VLS growth.

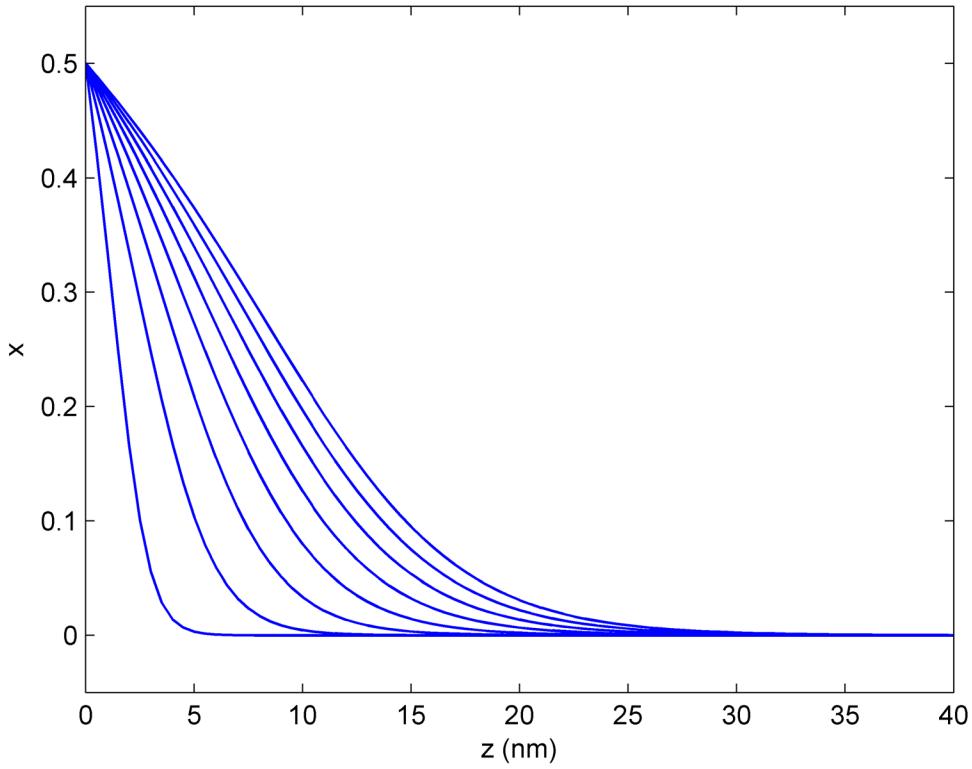

Figure 3. Calculated composition profiles of several trailing HJs as a function of the position along the growing direction *z* (NW axis). Each curve corresponds to one of the dashed lines of Figure 2, with the most abrupt profiles corresponding to initial conditions near the critical point.

3.2 Leading HJ

The leading HJ is the opposite of the trailing HJ, the NW growth is switched from Si to Si_xGe_{1-x}. In this case the system is located at a certain point below the Ge equilibrium curve (no Ge deposition), as a result only Si is being deposited in the solid phase (L + S(Si) equilibrium). Once the Ge source is switched-on, the Ge concentration in the liquid droplet increases up to supersaturation, then the system starts moving to the equilibrium curve of the target composition. The composition dynamics are the same as that of the trailing case, Eq. 5, but one has to take account of the dependence of C_{Ge} with the incoming Ge flux, ϕ_{Ge}. This term can be easily calculated because we know that the composition variation when the equilibrium curve is reached must be zero, i.e. $C_{Ge}^{i+1} = C_{Ge}^{i}$ and $\phi_{Ge} - x_0 \frac{3h}{d} = 0$, so it can be simply replaced by a term proportional to the final composition x_0

$$C_{Ge}^{i+1} = C_{Ge}^{i} + \phi_{Ge} - x_i(C_{Si}^{i}, C_{Ge}^{i})\frac{3h}{d} = C_{Ge}^{i} + (x_0 - x_i(C_{Si}^{i}, C_{Ge}^{i}))\frac{3h}{d} \qquad (7)$$

Si concentration C_{Si} follows Eq. 6.

The paths followed by the system are analogous to those of the trailing case but the system moves along them in the opposite direction, from the blue curve to the black one.

The simulated leading heterointerface profiles for a composition x = 0.5 are plotted in Figure 4 (same B and d values as for the trailing case, Figure 3), showing that also the leading heterointerface becomes sharper as the growth conditions approach the critical point.

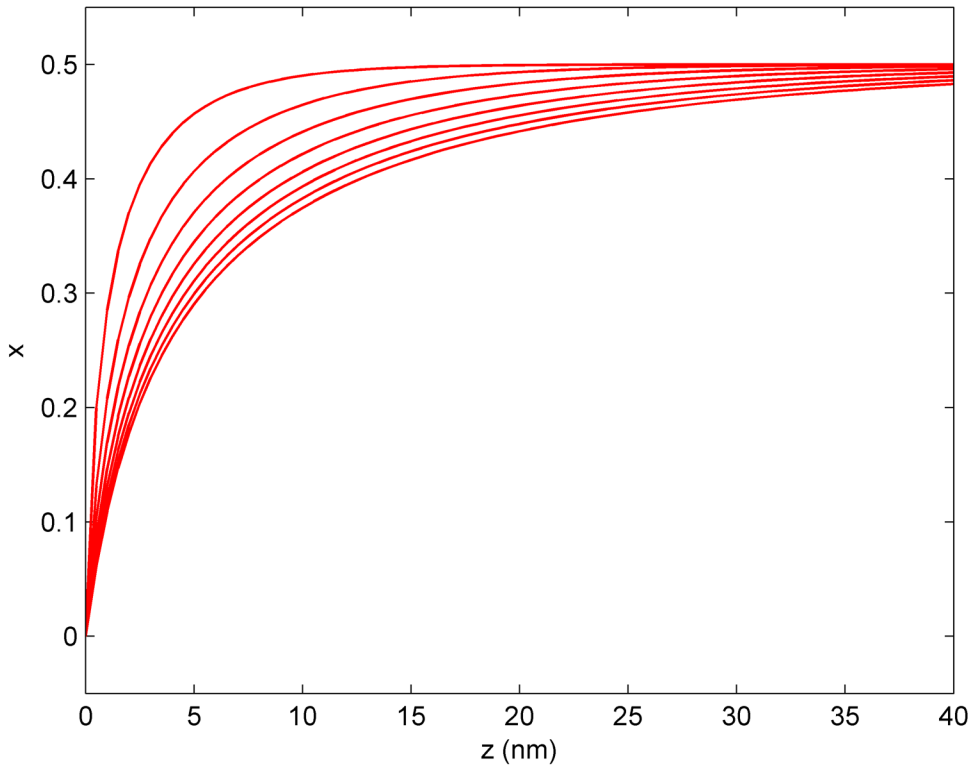

Figure 4. Composition profiles of several leading HJs as a function of the position along the growing direction (NW axis). Each curve corresponds to one of the dashed lines of Figure 2, with the most abrupt profiles corresponding to initial conditions near the critical point.

Note the different profiles of the trailing and leading heterointerfaces, consequence of the different starting points. While the reservoir effect governs the trailing interface, showing initially a slow decrease of the Ge concentration followed from a faster decrease, the leading heterointerface evidences a continuous increase of the Ge concentration. Note that both interfaces start from opposite situations, the trailing heterointerface departs from a Ge supersaturation situation, while the leading heterointerface starts from a Ge subsaturation situation, this difference results in distinct growth dynamics, therefore, distinct composition profiles across the heterointerface.

We have shown that the expected HJ widths are in both cases narrower than usually assumed. Figure 5 summarizes the data of Figures 3 and 4. It shows the leading and trailing HJ widths for B = 0.5 as a function of the Si concentration in the catalyst droplet, i.e. the initial position along the x = 0.5 curve. We see that both trailing and leading HJs become more abrupt as the initial state of the system approaches the critical point. Furthermore, close to the critical point both heterointerfaces present almost similar abruptness tending to zero, while departing away from the critical point, the heterointerfaces become more gradual. In all cases the trailing transition is more abrupt than the leading one, considering that the growth temperature and chamber pressure are kept constant, and the NW diameter does not change all along the growth run.

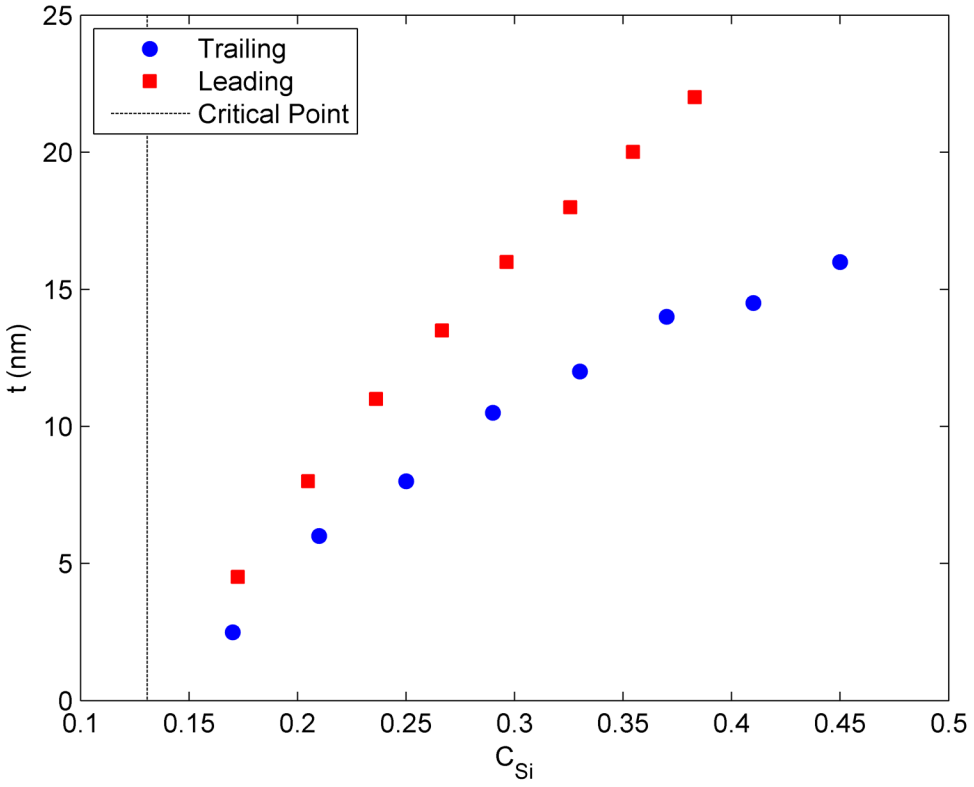

Figure 5. Widths of the trailing and leading HJs as a function of the initial Si concentration in the liquid droplet. The trailing HJ is sharper than the leading HJ for all

values of C_{Si}, and they converge at the critical point, which corresponds to an ideally abrupt transition for both interfaces.

On the other hand, Figure 6 summarizes the dependence of both leading and trailing heterointerfaces widths with respect to the B parameter. We see that for all values of B the trailing heterointerface is sharper than the leading one, assuming the same pressure and temperature conditions for both heterointerfaces. Moreover, we know that the values of B must be smaller than unity because of the higher solubility of Ge in Au, which results in HJ mean widths narrower than 30 nm according to Figure 6.

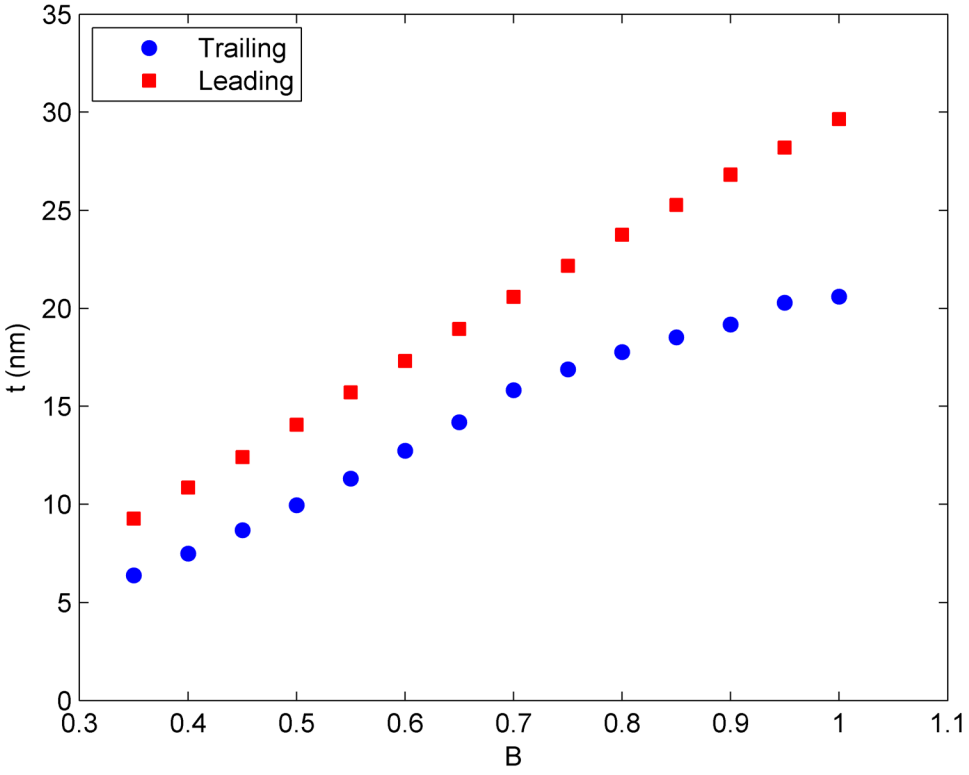

Figure 6. Trailing and leading HJ mean widths as a function of B parameter for x = 0.5 and d = 100 nm.

3. Experimental Measurements

In order to check the validity of the theoretical model energy dispersive X-ray spectroscopy (EDX) measurements have been carried out on SiGe/Si/SiGe heterostructured NWs.[31] For this, a field emission scanning electron microscope (FESEM) FEI Quanta 200FEG was used. The EDX profiles of the HJs allow us to have a measurement of the HJ width. However, these measurements have a great number of error sources. First, the electron beam drift due to charge localization in the NW can induce a relative error of up to 50% of the distance measured during the profile acquisition. Secondly, the electron beam diameter, which depends on several parameters, mainly on acceleration voltage and aperture size. For our experimental conditions, 10 kV, the expected beam diameter is ~ 4 nm. Furthermore, when the beam reaches the sample it broadens, in our experiment the beam is expected to change from 4 nm in the NW surface to ~ 6 nm on the opposite side of the NW, according to the material properties and NW diameter. The magnitude of the errors does not allow for a reliable measurement of the HJ width with these techniques. However, since the principal (and less controllable) source of errors is the beam drift we can still obtain qualitative information and check the validity of the modelled HJ profiles. If we rescale the distance of the EDX and backscattering scanning electron microscopy (SEM) profiles obtained from SiGe/Si/SiGe axially heterostructured NWs we can compare them with the theoretically calculated profiles, Figure 7.

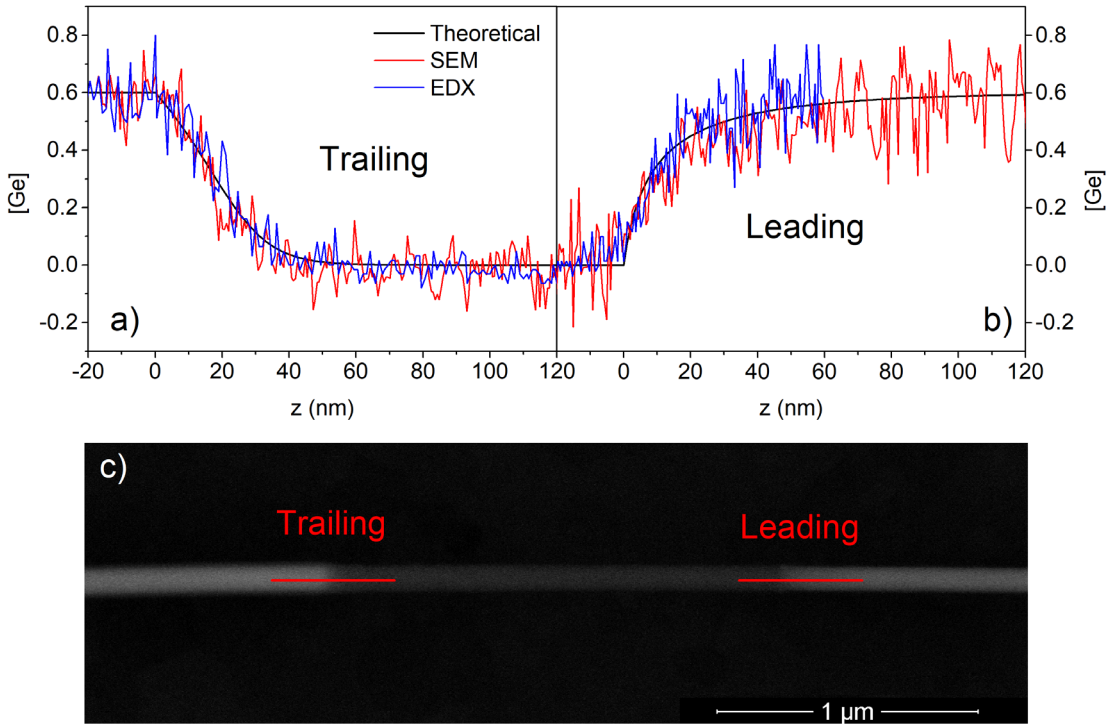

Figure 7. Rescaled backscattered SEM and EDX profiles of a trailing (a) and leading (b) HJs compared with the theoretically calculated profiles. c) Backscattering SEM image of a SiGe/Si/SiGe axially heterostructured NW (d ~ 100 nm) showing the trailing and leading HJs and the region of the profiles plotted in (a) and (b). It is important to note that the EDX profile is acquired in a continuous measurement for both trailing and leading HJ, this ensures that both are comparable even after the rescale process.

We see that the experimental measurements follow the theoretical profiles in both leading and trailing HJs, and also for the two types of recorded signals, backscattered SEM and EDX. All the analysed NWs presented similar profiles with only subtle variations and all of them followed the theoretical profiles. In all cases the trailing HJ appears to be sharper than the leading one. We should also note that two behaviours predicted by the model are observed in all the experimentally analysed NWs. First, the trailing HJ does not start with an exponential decay, but initially, in an extension of a few nanometres, a slower decrease is observed, later followed by an exponential decay. Second, an opposite effect is

observed in the leading HJ. Initially, the incorporation of Ge to the solid phase is faster, and near equilibrium it shows an exponential approximation to the composition target slower than initially expected. This effect appears as a result of the non-linearity of Eqs. 1-4. Further details about the profile shape can be found in the supporting information S2.

4. Discussion

It has been claimed that the Si/SiGe heterointerface width using Au catalyst droplets must have an extension equivalent to the NW diameter. This assertion is based on the reservoir effect, in which the Ge solved in the droplet continues to be deposited until exhaustion once the Ge flux was switched-off. Upon this mechanism, the extension of the graded heterointerface would be determined by the ratio between the droplet volume and the interface surface giving a graded interface width of around one diameter.[17] The reservoir effect must be reconsidered on the bases of the growth model developed here. In this model the Ge solved in the droplet is not exhausted, but it stops depositing once the equilibrium concentration of Ge in the droplet is reached, blue curve in Figure 2. This means that for the case represented in Figure 2 (x = 0.5), the deposited amount of Ge corresponds to the difference between the black and blue curves. Therefore, in the most unfavourable case a concentration fraction of ≈ 0.1 of Ge in the droplet is deposited, see the difference between the black and blue curves on the right side of Figure 2, while the rest of the Ge is under saturation and remains stored in the droplet.

If we balance the total Ge in the droplet that is deposited during the growth of the heterointerface, and the dimensions of the droplet and the heterointerface we can establish a simple relation between the heterointerface width and the diameter of the NW. Let

assume that the difference of Ge being in the droplet right before and after the compositional transition is the one deposited in the HJ region. The Ge deposited in the HJ must equal the Ge leaving the droplet, therefore, the density of Ge atoms in the droplet susceptible to be deposited (n_d) times the droplet volume should equal the mean density of Ge atoms in the HJ (n_{HJ}) times its volume. For the HJ region the mean value will be roughly half of the Ge concentration in the homogeneous segment, ~ 0.25 in this example. If *t* is the HJ thickness and d the droplet diameter the Ge conservation reads as

$$n_d V_d = n_{HJ} V_{HJ} \rightarrow 0.1 \frac{1}{2} \frac{4}{3} \pi r^3 = 0.25\, t\, \pi r^2 \rightarrow t = \frac{2r}{7.5} = \frac{d}{7.5} \qquad (8)$$

The HJ thickness is still proportional to the NW diameter, but the proportionality factor is sensitively smaller than unity. For a 100 nm NW we can see that the estimation, t = 13.33 nm, is in good agreement with the model calculations, Figure 5, also in good agreement with other experimental measurements. [32]

5. Conclusions

A systematic study of the VLS growth of axially heterostructured Si/SiGe NWs has provided information about the growth dynamics of axial heterojunctions. We show that both trailing and leading Si/SiGe heterojunctions can be narrower than usually claimed. Moreover, the existence of a critical point in the Au/Si/G alloy composition map shows a path to tailor the heterojunction width by changing the growth conditions (gas flows, temperature, pressure, etc). The heterojunction becomes narrower as the growing conditions approach the critical point. In practice, lowering both Si and Ge concentrations in the liquid droplet should allow to produce sharper heterojunctions. This is in good

agreement with the dynamics observed in III-V heterojunctions, where the low solubility of one of the constituents makes the abrupt heterointerfaces the natural process for those semiconductor NWs. In practice, the effect of selecting the growth conditions near the critical point, i.e. low Ge concentration, is equivalent to the natural low solubility of group V elements, a reduced amount of Ge in the droplet results in a more abrupt transition.[24] It also converges with the use of catalysts aiming to reduce the solubility of the atomic species.[14–16,32] Finally, the model results were compared with experimental measurements, obtaining a very good agreement from both quantitative and qualitative points of view.

Acknowledgements

This work was funded by Junta de Castilla y León (Projects VA293U13, and VA081U16), and Spanish Government (CICYT MAT2010-20441-C02 (01 and 02) and ENE 2014-56069-C4-4-R). J L Pura was granted by the FPU programme (Spanish Government) (FPU14/00916).

Supporting Information. Table with all the parameters used in the model. Logarithmic plot of the calculated heterojunction profiles showing the exponential and non-exponential behaviours of the growth mechanism.

References

(1) Li, Y.; Qian, F.; Xiang, J.; Lieber, C. M. Nanowire Electronic and Optoelectronic Devices. *Mater. Today* **2006**, *9* (10), 18–27.

(2) Thelander, C.; Agarwal, P.; Brongersma, S.; Eymery, J.; Feiner, L. F.; Forchel, A.; Scheffler, M.; Riess, W.; Ohlsson, B. J.; Gösele, U.; et al. Nanowire-Based One-Dimensional Electronics. *Mater. Today* **2006**, *9* (10), 28–35.

(3) Yan, R.; Gargas, D.; Yang, P. Nanowire Photonics. *Nat. Photonics* **2009**, *3* (10), 569–576.

(4) Boukai, A. I.; Bunimovich, Y.; Tahir-Kheli, J.; Yu, J. K.; Goddard, W. A.; Heath, J. R. Silicon Nanowires as Efficient Thermoelectric Materials. *Nature* **2008**, *451* (7175), 168–171.

(5) Jebril, S.; Kuhlmann, H.; Müller, S.; Ronning, C.; Kienle, L.; Duppel, V.; Mishra, Y. K.; Adelung, R. Epitactically Interpenetrated High Quality ZnO Nanostructured Junctions on Microchips Grown by the Vapor-Liquid-Solid Method. *Cryst. Growth Des.* **2010**, *10* (7), 2842–2846.

(6) Pötz, W.; Li, Z. Q. Imperfections and Resonant Tunneling in Quantum-Well Heterostructures. *Solid. State. Electron.* **1989**, *32* (12), 1353–1357.

(7) Cosentino, S.; Mio, a M.; Barbagiovanni, E. G.; Raciti, R.; Bahariqushchi, R.; Miritello, M.; Nicotra, G.; Aydinli, A.; Spinella, C.; Terrasi, A.; et al. The Role of the Interface in Germanium Quantum Dots: When Not Only Size Matters for Quantum Confinement Effects. *Nanoscale* **2015**, *7* (26), 11401–11408.

(8) Wagner, R. S.; Ellis, W. C. Vapor-Liquid-Sold Mechanism of Single Crystal Growth. *Appl. Phys. Lett.* **1964**, *4* (5), 89–90.

(9) Dick, K. A.; Deppert, K.; Larsson, M. W.; Mårtensson, T.; Seifert, W.; Wallenberg, L. R.; Samuelson, L. Synthesis of Branched "Nanotrees" by Controlled Seeding of Multiple Branching Events. *Nat. Mater.* **2004**, *3* (6), 380–384.

(10) Lauhon, L. J.; Gudiksen, M. S.; Lieber, C. M. Semiconductor Nanowire Heterostructures. *Philos. Trans. R. Soc. A* **2004**, *362* (1819), 1247–1260.

(11) Gudiksen, M. S.; Lauhon, L. J.; Wang, J.; Smith, D. C.; Lieber, C. M. Growth of Nanowire Superlattice Structures for Nanoscale Photonics and Electronics. *Nature* **2002**, *415*, 617–620.

(12) Borgström, M. T.; Verheijen, M. A.; Immink, G.; De Smet, T.; Bakkers, E. P. A. M. Interface Study on Heterostructured GaP-GaAs Nanowires. *Nanotechnology* **2006**, *17*, 4010–4013.

(13) Zakharov, N. D.; Werner, P.; Gerth, G.; Schubert, L.; Sokolov, L.; Gösele, U. Growth Phenomena of Si and Si/Ge Nanowires on Si (1 1 1) by Molecular Beam Epitaxy. *J. Cryst. Growth* **2006**, *290* (1), 6–10.

(14) Geaney, H.; Mullane, E.; Ramasse, Q. M.; Ryan, K. M. Atomically Abrupt Silicon-Germanium Axial Heterostructure Nanowires Synthesized in a Solvent Vapor Growth System. *Nano Lett.* **2013**, *13* (4), 1675–1680.

(15) Wen, C. Y.; Reuter, M. C.; Bruley, J.; Tersoff, J.; Kodambaka, S.; Stach, E. A.; Ross, F. M. Formation of Compositionally Abrupt Axial Heterojunctions in Silicon-Germanium Nanowires. *Science (80-.).* **2009**, *326* (5957), 1247–1250.

(16) Chou, Y. C.; Wen, C. Y.; Reuter, M. C.; Su, D.; Stach, E. A.; Ross, F. M. Controlling the Growth of Si/Ge Nanowires and Heterojunctions Using Silver-

Gold Alloy Catalysts. *ACS Nano* **2012**, *6* (7), 6407–6415.

(17) Li, N.; Tan, T. Y.; Gösele, U. Transition Region Width of Nanowire Hetero- and Pn-Junctions Grown Using Vapor – Liquid – Solid Processes. *Appl. Phys. A Mater. Sci. Process.* **2008**, *90*, 591–596.

(18) Pura, J. L.; Anaya, J.; Souto, J.; Prieto, Á. C.; Rodríguez, A.; Rodríguez, T.; Jiménez, J. Local Electric Field Enhancement at the Heterojunction of Si/SiGe Axially Heterostructured Nanowires under Laser Illumination. *Nanotechnology* **2016**, *27* (45), 455709.

(19) Pura, J. L.; Anaya, J.; Souto, J.; Prieto, A. C.; Rodríguez, A.; Rodríguez, T.; Periwal, P.; Baron, T.; Jiménez, J. Electromagnetic Field Enhancement Effects in Group IV Semiconductor Nanowires. A Raman Spectroscopy Approach. *J. Appl. Phys.* **2018**, *123* (11), 114302.

(20) Periwal, P.; Bassani, F.; Patriarche, G.; Latu-Romain, L.; Brouzet, V.; Salem, B.; Baron, T. Interfacial Abruptness in Axial Si/SiGe Heterostructures in Nanowires Probed by Scanning Capacitance Microscopy. *Phys. Status Solidi Appl. Mater. Sci.* **2014**, *211* (2), 509–513.

(21) Periwal, P.; Baron, T.; Latu-romain, L.; Salem, B.; Patriarche, G.; Gentile, P. Control of the Interfacial Abruptness of Au-Catalyzed Si-Si1-xGex Heterostructured Nanowires Grown by Vapor-Liquid-Solid. *J. Vac. Sci. Technol. A Vacuum, Surfaces, Film.* **2014**, *32* (3), 31101.

(22) Chou, Y. C.; Hillerich, K.; Tersoff, J.; Reuter, M. C.; Dick, K. A.; Ross, F. M. Atomic- Scale Variability and Control of III- V Nanowire Growth Kinetics. *Science (80-.).* **2014**, *343*, 281–284.

(23) Gamalski, A. D.; Ducati, C.; Hofmann, S. Cyclic Supersaturation and Triple Phase Boundary Dynamics in Germanium Nanowire Growth. *J. Phys. Chem. C* **2011**, *115* (11), 4413–4417.

(24) Wen, C.-Y.; Tersoff, J.; Reuter, M. C.; Stach, E. A.; Ross, F. M. Step-Flow Kinetics in Nanowire Growth. *Phys. Rev. Lett.* **2010**, *105* (19), 195502.

(25) Wang, H.; Zepeda-Ruiz, L. A.; Gilmer, G. H.; Upmanyu, M. Atomistics of Vapour-Liquid-Solid Nanowire Growth. *Nat. Commun.* **2013**, *4*, 1956.

(26) Wacaser, B. A.; Dick, K. A.; Johansson, J.; Borgström, M. T.; Deppert, K.; Samuelson, L. Preferential Interface Nucleation: An Expansion of the VLS Growth Mechanism for Nanowires. *Adv. Mater.* **2009**, *21* (2), 153–165.

(27) Glas, F. Chemical Potentials for Au-Assisted Vapor-Liquid-Solid Growth of III-V Nanowires. *J. Appl. Phys.* **2010**, *108* (7), 73506.

(28) Stringfellow, G. B. Calculation of Ternary Phase Diagrams of III-V Systems. *J. Phys. Chem. Solids* **1972**, *33* (3), 665–677.

(29) Massalski, T. B. *Binary Alloy Phase Diagrams*, 2nd ed.; ASM International: Metals Park: Ohio, 1990.

(30) Clark, T. E.; Nimmatoori, P.; Lew, K.; Pan, L.; Redwing, J. M.; Dickey, E. C. Diameter Dependent Growth Rate and Interfacial Abruptness in Vapor – Liquid – Solid Si / Si 1 - X Ge X Heterostructure Nanowires. *Nano Lett.* **2008**, *8* (4), 1246–1252.

(31) Periwal, P.; Sibirev, N. V.; Patriarche, G.; Salem, B.; Bassani, F.; Dubrovskii, V. G.; Baron, T. Composition-Dependent Interfacial Abruptness in Au-Catalyzed Si1−xGex/Si/Si1−xGex Nanowire Heterostructures. *Nano Lett.* **2014**, *14*, 5140–

5147.

(32) Perea, D. E.; Li, N.; Dickerson, R. M.; Misra, A.; Picraux, S. T. Controlling Heterojunction Abruptness in VLS-Grown Semiconductor Nanowires via in Situ Catalyst Alloying. *Nano Lett.* **2011**, *11* (8), 3117–3122.